

Determining lateral offsets of rocks along the eastern part of the North Anatolian Fault Zone (Turkey) using spectral classification of satellite images and field measurements

Önder Gürsoy ^a, Şinasi Kaya ^b, Ziyadin Çakır  ^c, Orhan Tatar  ^d and Oktay Canbaz  ^d

^aDepartment of Geomatics Engineering, Cumhuriyet University, Sivas, Turkey; ^bDepartment of Geomatics Engineering, Istanbul Technical University, Istanbul, Turkey; ^cDepartment of Geological Engineering, Istanbul Technical University, Istanbul, Turkey; ^dDepartment of Geological Engineering, Cumhuriyet University, Sivas, Turkey

ABSTRACT

Fault displacements are being measured by geological observations using the method of detecting and evaluating marker rocks. Thus, the length of total displacement in a fault zone relates to position detection of marker rocks. Due to limits of human eye, we used remote sensing data and terrestrial spectral measurements at 229 locations for measuring the total offset along the Kelkit Valley segment of the North Anatolian Fault Zone (NAFZ). We examined the lithology, especially ophiolites that are older than the fault zone and can be a good marker for detecting the total offset in the region. The Advanced Spaceborne Thermal Emission and Reflection Radiometer images are subjected to Spectral Angle Mapper (SAM) method. Principal component analysis, decorrelation stretching and geological map were used to compare the SAM results. Ophiolites on either side of the fault zone were clearly classified and identified with the SAM analysis. As a result of comparison of SAM with image enhancement methods and the geological map, we measured the total fault displacement on the NAFZ in the part of the Kelkit Valley. Along the fault zone to the north and south of the ophiolites providing a right lateral offset was measured as 90 ± 5 km.

ARTICLE HISTORY

Received 21 December 2016

Accepted 10 April 2017

KEYWORDS

NAFZ; total offset; remote sensing; spectral classification

1. Introduction

Depending on the tectonic activities such as crustal deformations and earthquakes, displacements in the fault zones have been ongoing since millions of years. Determining the cumulative slip and measuring the offset along the fault zones are important for identifying the crustal deformation. Kelkit Valley segment is one of the zones that is exposed to many tectonic activities along the North Anatolian Fault Zone (NAFZ) and last ruptured in 1939 (Figure 1(a)). Determining the total displacement that have been caused by the tectonic activities on the NAFZ, many geological researches (Ketin 1948; Seymen 1975; Tatar 1975; Tatar 1978; Şengör 1979; Sipahioglu 1984; Şengör et al. 1985; Saroğlu 1988; Nurlu et al. 1995; Tatar 1996a, b; Yaltırak et al. 1998; Armijo et al. 1999; Yaltırak et al. 2000; Ayhan et al. 2001; Akyüz 2002; Özalaybey et al. 2002; Yaltırak 2002; Şengör et al. 2005; Tatar et al. 2006; Tatar et al. 2012) have been made since the right lateral strike-slip definition of the fault zone. The total displacement on the NAFZ has been identified by detecting and evaluating the marker rocks. Şengör et al. (1985) pointed out that the cumulative offset of the NAFZ has long been a contentious issue. For many years, Seymen's (1975) estimate of the dextral offset of the Ankara–

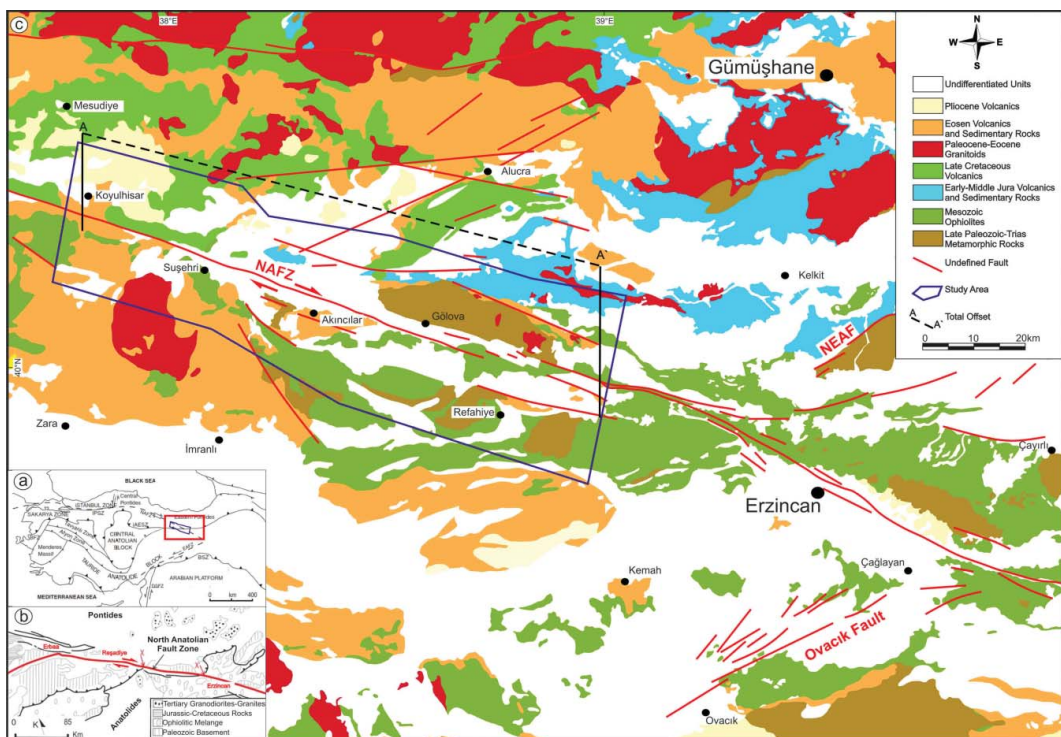


Figure 1. (a) Neotectonic elements of Turkey (Okay & Tüysüz 1999). (b) Geological map shows the offset of suture zone (barbed lines) along the NAFZ, Erzincan-Resadiye (Seymen 1975; Şengör et al. 1985). The offset between X and X' along the fault is 85 ± 5 km. (c) The geological map of the study area (revised by using the maps of General Directorate of Mineral Research and Exploration of Turkey (MTA)).

Erzincan suture zone for some 85 ± 5 km was taken as the offset, although Şengör (1979) pointed out as early as 1979 that the total displacement along the fault was less in the west than it was in the east. Bergougnan's (1976) mapping revealed a similar offset in the same region as Seymen's offset. Seymen's estimate was disputed by others working on different parts of the entire NAFZ (e.g. Barka 1981, 1992; Şaroğlu 1988; Koçyiğit 1988, 1989), but none of these authors addressed the problem of multiple parallel faults and other structures that also take up displacement in the North Anatolian Shear Zone (NASZ). Indeed, the faults named as 'splay faults' branching out from the main NAFZ around the southern edge of the Niksar-Erbaa basin into the Anatolian block accommodate some of the displacement in the NASZ. This is also proved by palaeomagnetic studies within the splay fault system of the NAFZ located to the west of Tokat and Amasya (Tatar et al. 1996). Şengör et al. (2005) believe that there is a genuine problem with Seymen (1975)'s estimate that only became known after it was discovered that considerable strike-slip faulting before the origin of the NASZ may have displaced the continental margin on which they had measured the offset. First, Yilmaz et al. (1993) showed that there probably was significant strike-slip faulting, most likely dextral, along the future site of the NAFZ between Havza and Niksar. Second, Cretaceous melanges have been found mainly within the pre-Liassic body of Tokat Massif along narrow zones (Bozkurt et al. 1997) that are probably of strike-slip nature. If so, Şengör et al. (2005) agree that these would have displaced the southern margin of the Tokat Massif, Seymen's marker 's' of the NAFZ, before the NAFZ formed. Surprisingly, Seymen's figure of 85 ± 5 km still seems to be in good agreement with the more recent estimates measured on more reliable markers. Herece and Akay (2003) tabulated all the former estimates of total offset along the NAF (except those in Hubert-Ferrari et al. 2002, 2009), which range from 7.5 km to 300–400 km. Their own estimates on the basis of data displayed in

Herce and Akay (2003) range from 7 to 155 km. Şengör et al. (2005) do not agree that all of the markers they used are equally reliable.

The same applies to Hubert-Ferrari et al. (2002) estimates of maximum offset. For instance, their reported offset of the ‘two sheared folds’ between the Tosya and the Vezirköprü basins cannot be substantiated in the field because the ‘matchable’ features give offsets of only 13 ± 1 km. But Hercce and Akay (2003)’s matching also is not reliable because on both sides of the NAFZ, similar units are folded in a similar style and it is arbitrary with which ‘southern fold’ one wishes to correlate a ‘northern fold.’ This shows the great dangers of mapping from space images and only cursory field checks, without producing detailed geological maps (Şengör et al. 2005). Moreover, to estimate the total displacement on the zone, measuring crustal movement with Global Positioning System (GPS) (Blewitt 1993) was used. Depending on the age of the fault, average slip rate measured by GPS on the zone is used for estimation of the total displacement. Geological and geodetic studies have shown that the total horizontal offset on the NAFZ is 85 ± 5 km, as revealed by the offset on tectonic suture shown in Figure 1(b) (Seymen 1975; Şengör 1979). Structural signs in big riverbeds and deformation boundaries also support this 85 ± 5 km displacement (Hubert-Ferrari et al. 2002). Along with studies towards the determination of the age of NAFZ, there have been studies to determine the total throw in the zone as well. The age of the fault zone was stated as Pliocene by Abdüsselamoğlu (1959) and Tatar (1975), Early Pliocene by Kocyigit (1989), Late Miocene by Nebert (1962) and Tatar (1978), Middle Miocene by Ketin (1976) and Miocene by Bozkurt (2001).

Geodetic data can provide detailed spatial coverage but represent only the short time interval of a single earthquake cycle, while geologic rates are derived as average values for multiple events at spatially limited sites where cumulative offsets have been preserved. Geodetic and geologic rates together provide a deeper understanding of the spatial and temporal behaviours of fault systems, especially in complex structural settings (Zabci et al. 2015) such as the NAFZ.

Velocity profiles on the NAFZ, based on more closely spaced GPS measurements, indicate eastwardly decreasing slip rates from 24.0 ± 2.9 to 16.2 ± 2.3 mm/year, in contradiction to the spatially constant rate published by Reilinger et al. (2006) between Niksar in the west and Erzincan in the east (Tatar et al. 2012).

However, interferometric synthetic aperture radar (InSAR)-based velocity profiles show relatively constant rates of, from west to east, 20 ± 3 mm/year (between longitudes 36.4°E and 38.8°E) (Çakir et al. 2014), 20–26 and 20 ± 3 mm/year (between Niksar and Erzincan) (Walters et al. 2011, 2014), and 20 mm/year (west and east of Erzincan) (Cavalié & Jónsson 2014) for the same central-to-eastern parts of the NAFZ, except for a slight decrease near the Karlıova Triple Junction (Zabci et al. 2015). This suggests the localization of most of the strain along the NAFZ, which acts as a plate boundary (Cavalié & Jónsson 2014).

The marker rocks that are used for determining the total displacement on fault zones could be detected by using remote sensing images. By uncovering the spectral signatures of multispectral images, it is possible to distinguish and map hundreds of different minerals and mineral assemblages. Actions of common geological processes over time on landforms are usually defined on the basis of homogeneous terrain characteristics (Hammond 1964; Dikau 1989; Bolongaro-Crevenna et al. 2005; Kruse 2012; Kruse & Perry 2013). Moreover, the relationships among the lithology of the bedrocks and soils of their surfaces and the chemically reactivity with the surface soil in the minerals can be classified (Vicente & Filho 2011). One of the most popular spectral classification methods that uses the remotely sensed data and spectral measurement is Spectral Angle Mapper (SAM) that was used for classifying mineral classes of the collected endmembers from the Advanced Spaceborne Thermal Emission and Reflection Radiometer (ASTER) satellite shortwave infrared (SWIR) bands (Kruse & Perry 2013). ‘An advantage of ASTER data is the unique combination of wide spectral coverage and high spatial resolution in the visible near-infrared through short-wave infrared to the thermal infrared regions. Hence, these data enhance the capability of lithological discrimination between the different rock units. Because of this advantage, ASTER simulation and data have been used increasingly for geological mapping’ (Okada & Ishii 1993; Bedell 2001; Abdeen et al. 2001;



Velosky et al. 2003; Rowan & Mars 2003; Hewson et al. 2005; Rowan et al. 2005; Gad & Kusky 2007; Gursoy & Kaya 2016).

In this study, SAM was employed which enables spectral classification in recognizing lithological and mineralogical structures. In order to be eligible for comparison with the SAM results, ASTER images were subjected to the enhancement methods for consideration the similarities and differences. The principal components transformation, which is one of these enhancement methods, is useful in visual interpretation (to determine hydrothermal alteration minerals) and determination of surface materials (Sing & Harrison 1985; Kaya 1999; Kariuki et al. 2003; Khan & Gleen 2006; Massironi et al. 2008; Natraj et al. 2010). As a result, total displacement along the fault zone was obtained based on the lithology of the geological units revealed.

The objective of this study is to analyze the relative positions of geological structures in the fault zone by determining the mineralogical and geological structures using remote sensing and geodetic studies along the Kelkit Valley segment of the NAFZ, which is one of the most important strike-slip faults in the world and has caused destructive earthquakes during the years of 1939 (Erzincan Ms = 7.9), 1942 (Niksar-Erbaa, Ms = 7.1) and 1992 (Erzincan, Ms = 6.8) (Tatar et al. 2012).

The study region is located along the Kelkit Valley on the NAFZ (Figure 1(c)). The region with the main faults that are NAFZ, Northeast Anatolian Fault (NEAF) and Ovacik Fault (OF) contains tectonic features such as earthquakes (Ketin 1976; Barka & Kadinsky-Cade 1988; Tatar et al. 2012). Several strike-slip-related sedimentary basins cause the crustal movement in the region (Kaypak & Eyidogan 2002). And, the serpentinite, one of the basement rocks in the region, is cut by these faults. It reflects many tectonic characteristics.

2. Materials and methods

Nine frame images of ASTER SWIR bands were acquired as remote sensing data for this study (Table 1). The geological maps obtained from the General Directorate of Mineral Research and Exploration of Turkey were revised by the authors. Spectral signatures of the rocks at 229 locations were measured. The satellite images and geological data were defined in the 37th North zone in World Geodetic System 1984 (WGS 84) datum of the Universal Transverse Mercator (UTM) projection system.

Correcting the leakage of photons from one detector element to another, cross-talk adjustment (Iwasaki et al. 2001; Iwasaki & Tonaka 2005) was utilized to ASTER images. Correcting atmospheric transmission and anthropogenic effects, the satellite sensor data used in the study were subjected to radiance calibration and reflectance conversion from radiance through atmospheric adjustment process in order to enhance utility. Through the application of atmospheric rectification on satellite data, satellite data are enabled to be processed in the same environment of spectroradiometer measurement data where no atmospheric effect is present (Kaya et al. 2004; Kruse 2012). Atmospheric rectification of the satellite image used in the present study was carried out on the basis of the values calculated through the Moderate resolution Transmission Model (MODTRAN) algorithm (Thome et al. 2001).

Table 1. ASTER images.

ASTER ID	Path/row/swath	Acquisitions dates (year/month/day)
AST3A1 0608280813430810110996	172/94/2	2006/08/28
AST3A1 0608030819580810110994	173/94/4	2006/08/03
AST3A1 0608030819490810100948	173/93/4	2006/08/03
AST3A1 0605220825330812171049	174/93/4	2006/05/22
AST3A1 0508160819210810091017	173/93/1	2005/08/16
AST3A1 0505100831510809261070	175/92/5	2005/05/10
AST3A1 0310050826050708010053	174/93/6	2003/10/05
AST3A1 0208310827320812171050	174/92/3	2002/08/31
AST3A1 0208310827410412120887	174/93/3	2002/08/31

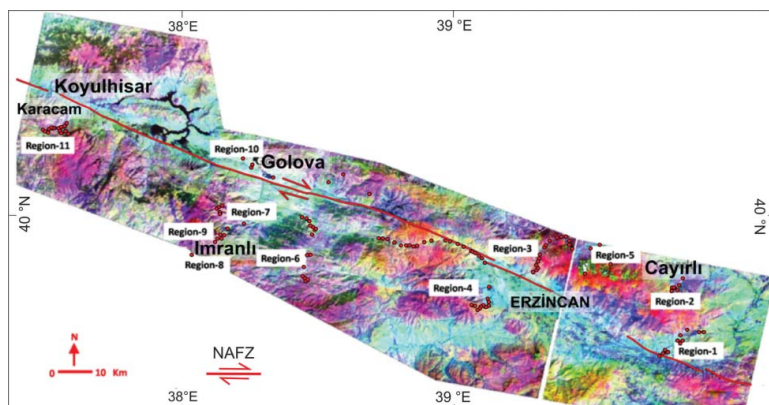


Figure 2. The presentation of 229 spectroradiometer measurement points in the 11 test region, on decorrelation stretching image (red dots show field spectroradiometer measurement locations). (To view this figure in colour, please see the online version of the journal.)

Due to the size of the study area, a decorrelation stretching analysis was used to determine the 11 test areas which contain serpentine as a marker rock. The serpentine outcrops were detected with the field observations in the areas. In June 2009, Analytical Spectral Devices (ASD) Fieldspec Pro spectroradiometer measurements within the scope of the study were performed at 11 test areas (229 points). Spectral measurements were carried out *in situ* 10 times for each rock sample with self-illuminated contact-probe lens. The average values of these measurements were used to determine the rock groups and to reveal the geological units (Figure 2). In order to match the enhanced images and the geological map used in the study, coordinate of each point was recorded by a handheld GPS and the types of rocks on which the measurements were done.

As belonging to the serpentinite having the best fit of spectral signature of 26 spectral measurements used as endmember, the spectral data os123, os124, os125 measured in Çayırı region, os11, os12, os13, os14 measured in İmranlı region and os182, os183, os184, os185, os186, os187, os188, os189, os190, os191, os192, os193, os194 and os195 measured along Erzincan–Sivas highway were used. Averages of these measurements were taken for each region. Afterwards, resampling of spectroradiometer measurements of the ophiolites in three different regions to ASTER SWIR bands was made. The three resampled spectra of ophiolites were averaged for determining general spectra of endmember. Comparing the general spectra of endmember with the Spectral Library of the United States Geological Survey (USGS), two different spectra of serpentinite from the library were used. According to the comparison, the general endmember spectra were compatible with the spectra of serpentinites from the Spectral Library of USGS (Figure 3).

The geological maps that have the layers with feature information of each formation age, ground structure and symbol codes, and the vectoral properties of the formation that are known, were rearranged according to unit ages. In this arrangement, each of their age was assigned a different colour code of R–G–B (Figure 1(c)).

Determining the total displacement in Kelkit Valley segment of the NAFZ, SAM classification method was used. Because serpentinite is older than the NAFZ in the region, serpentinite were selected as the endmember of marker rock. Comparing the SAM result, image enhancement methods such as decorrelation stretching and principal component analysis (PCA) were used.

2.1. SAM spectral classification

Detecting the locations of the ophiolites that are used as endmember, SAM classification method was performed for nine scenes of ASTER images. The average spectral angle for an endmember

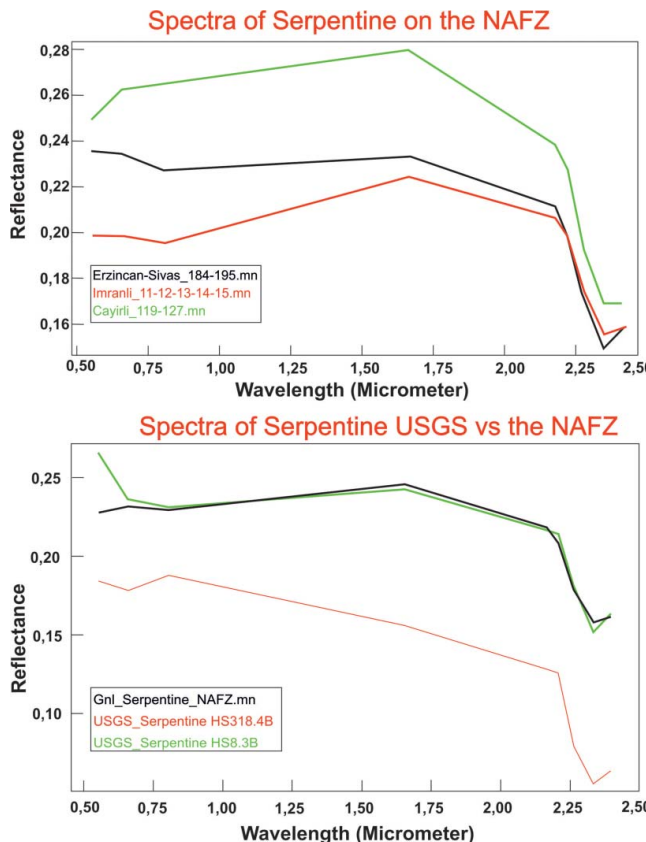


Figure 3. (a) Resampling of spectroradiometer measurements of serpentinite in three different regions to ASTER SWIR bands. The spectra of serpentinite were averaged for every region. Each colour of average spectra represents a different region. Black spectra: the averages of spectroradiometer measurements for Erzincan–Sivas highway (measurements from os182 to os195). Red spectra: Imranli (measurements from os11 to os14) and green spectra: Cayirli (measurements from os119 to os127). (b) Averaged spectra of serpentinite that was measured in three different regions on the NAFZ and two spectra of serpentinite from USGS Spectral Library. (To view this figure in colour, please see the online version of the journal.)

modelling its own class using SAM was calculated with the formula which was used in Dennison et al. (2004). In SAM, 0.075 radian was assigned as optimal threshold value for endmember of ophiolite (Figure 3). According to the SAM, we detected ophiolites, which could be used for displacement analysis, in two of the nine frames (AST3A10310050826050708010053 and AST3A10508160819210810091017) of ASTER images (Figure 4).

2.2. Image enhancement methods

The image enhancement analysis of PCA and decorrelation stretching were used for visualization of the lithology. It is impossible to determine the objects by using the enhancement analysis. Because of this, a reference data have to be used for determining the objects of the classes. The geological map was used as reference data for identifying the lithology.

PCA image enhancement technique image enables more than 90% of the data contained by all bands to be shown in the first three components by reducing the correlation between the bands. For the first three components in PCA image, R was displayed as the first component while G and B were displayed, respectively, as the second and the third components (Figure 5(a)).

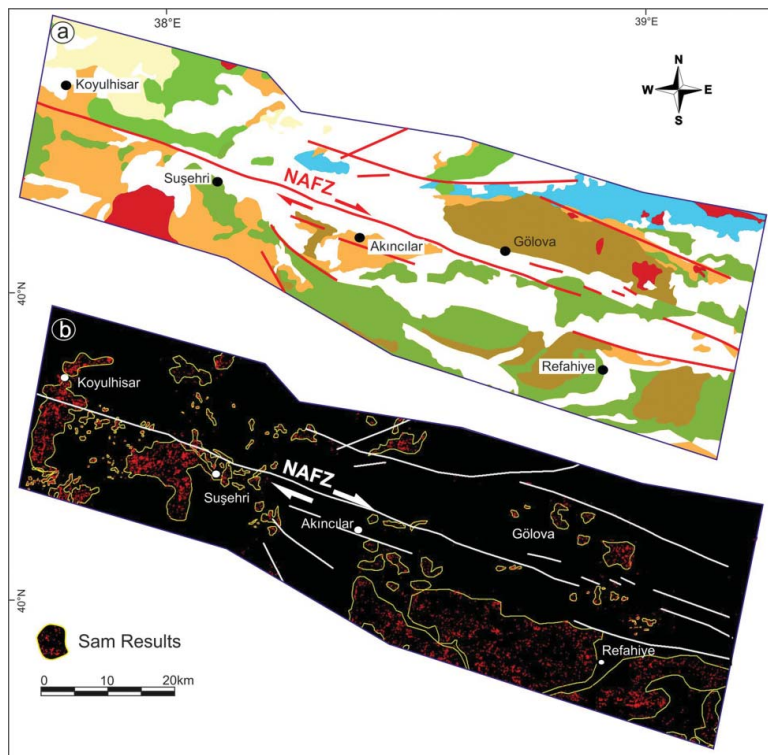


Figure 4. (a) The geological map. (b) SAM results, the contributions of the endmember of marker rocks (every red colour of pixel is an endmember of ophiolitic in yellow polygons) in the north and south sides of the NAFZ. (To view this figure in colour, please see the online version of the journal.)

Decorrelation stretching, which is one of the image enhancement methods, and principal components transformation methods were applied to the ASTER satellite images. The satellite image data interpretability was increased by applying enhancement methods which were then analyzed to sort out geological structures as well as to determine regions of geodetic spectral measurements. Decorrelation stretching was applied to 9–7–4 SWIR bands of nine ASTER satellite frame images obtained in the context of the study. Before the decorrelation stretching analysis, the band combination having the lowest correlation was selected by checking the correlation among the bands (R: SWIR-9, G: SWIR-7 and B: SWIR-4 bands) (Figure 5(b)).

3. Results of fault displacement analysis

In order to determine the total fault displacement, which was mentioned in Figure 1, on the NAFZ, we identified the locations of the ophiolites that were used as marker endmember with SAM classification method. According to the SAM, the similarities in northwestern and southeastern parts of the NAFZ were analyzed. The regions in the south and north of the NAFZ where endmember belonging to serpentinite were determined in SAM analysis image. Serpentinite endmember on the south of the NAFZ is located around Koyulhisar and that on the north of the NAFZ is located around Gölova.

Rock types of the ophiolites that were used in SAM were verified by comparing to the spectral signatures of the serpentinites in the USGS Spectral Library (Figure 3). Three different types of serpentinite that were collected at three different locations were averaged to be used in SAM.

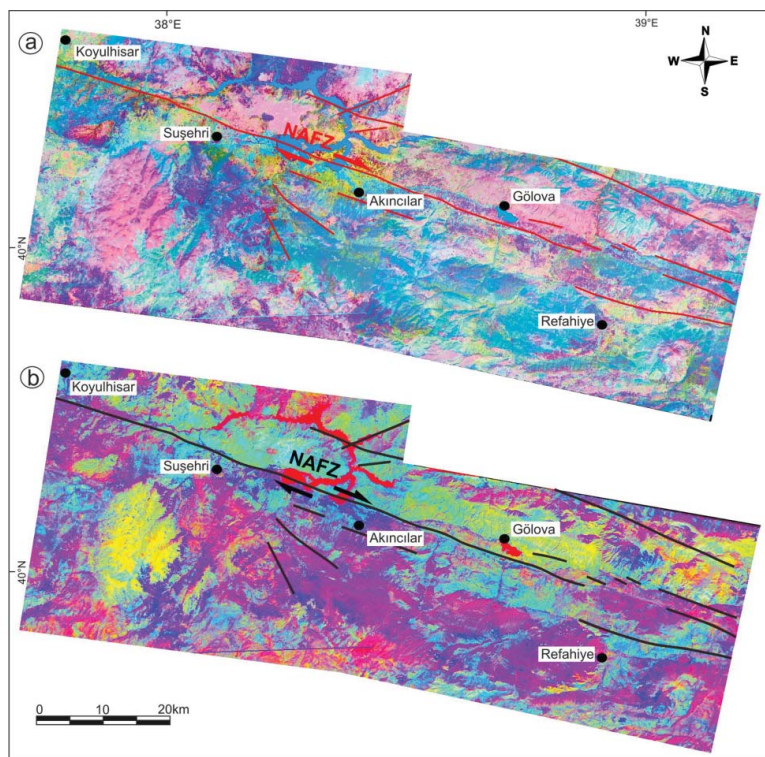


Figure 5. (a) Principal components transformation resulting image composite (K: first component, Y: second component, M: third component) and the NAFZ. (b) Decorrelation stretch image (R: SWIR 9; G: SWIR 7; B: SWIR 4) and the NAFZ (black lines). (To view this figure in colour, please see the online version of the journal.)

Figure 4 shows the distributions of the serpentinite endmember that was used in SAM on the NAFZ. As the SAM analysis result was analyzed, it is seen that the serpentinite endmember is available in the north and south of the NAFZ. Moreover, there are areas where SAM analysis conforms to the geological map.

For visualizing the part of the NAFZ and comparing the SAM, image enhancement analysis was used. According to the PCA image and decorrelation stretching image in Figure 6, contributions of the ophiolites on the NAFZ were compatible with the SAM results.

As a result of the SAM and comparison of the SAM with image enhancement methods and the geological map, we measured the total fault displacement on the NAFZ in the part of the Kelkit Valley. The result of the 90 ± 5 kilometers of total displacement on the Kelkit Valley part of the NAFZ is shown in Figure 6. The result is consistent with previous researches that are mentioned in Figure 1(b) (Seymen 1975; Şengör 1979). Due to the spatial resolution of the ASTER images, small scale of serpentines which were observed close to A and A' were not classified. According to the distance of the unclassified serpentines, the ± 5 km error of the result was measured.

4. Discussions and conclusion

This paper aims to determine the endmember of marker rocks in the central-eastern part of the NAFZ and measure the distance between endmember in the north and south sides of the NAFZ. Because of its age that is older than the age of the NAFZ, ophiolitic rocks were used as marker. For measuring spectral signatures of the marker rocks, we determined 11 different test regions in the south and north sides of the NAFZ on the Kelkit Valley segment of the

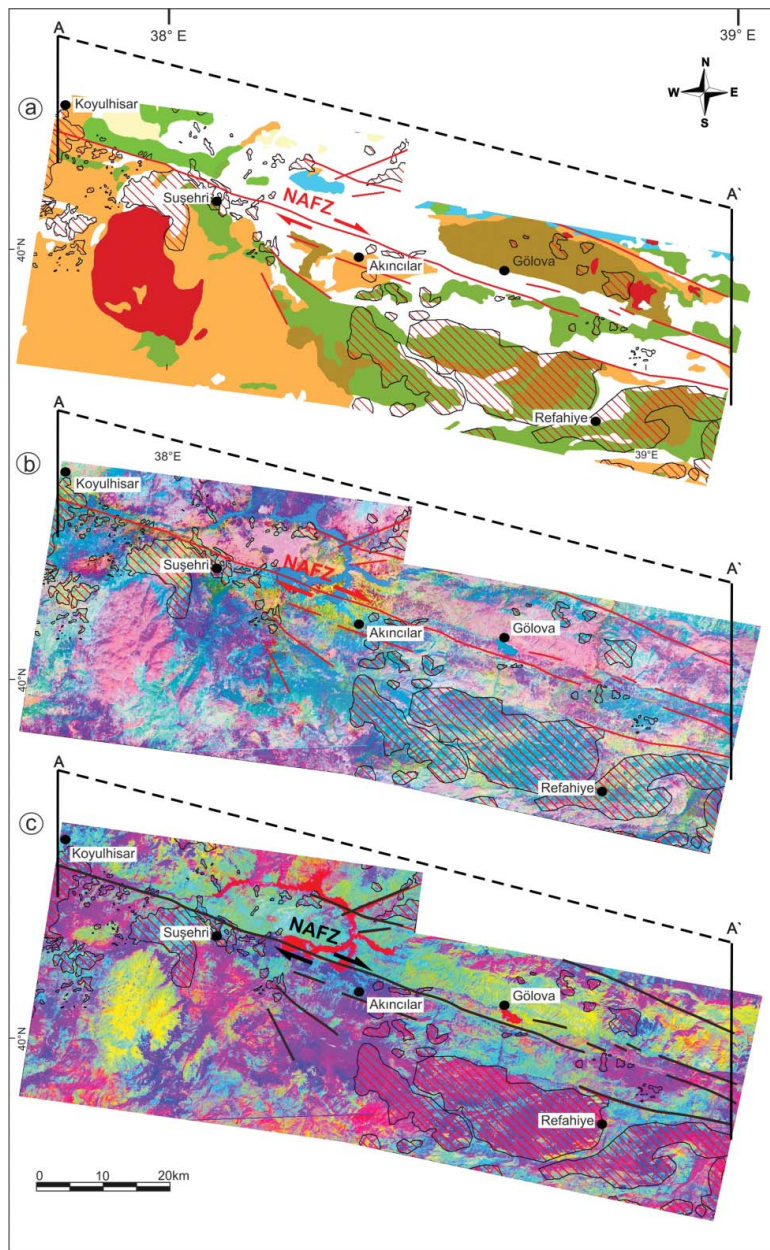


Figure 6. The representation of serpentinite endmembers in SAM analysis image. The serpentinite endmember which is used in SAM classification was shaded red polygons. Contributions of the rocks in red shaded areas are compatible with the geological map (a), PCA (b) and decorrelation stretching. (c) The fault displacement determined and measured in the study region along A–A'. The distance between A and A' is (90 ± 5) km, which is in conformity with the distance between X and X' shown in Figure 1(b) on the geological map. (To view this figure in colour, please see the online version of the journal.)

NAFZ. At 229 different locations, we measured the spectral signatures of the rocks. We detected ophiolites in three regions to be used in classification. The ophiolitic rocks of end-member in the Çayırlı region, İmranlı region and along the Erzincan–Sivas highway were used. The general averaged spectra of the rocks that were from the three regions were used in SAM as endmember.



The analysis done for the displacement showed that the existence of similar geological units on the north and south of the fault on the NAFZ is evident in terms of lithological aspects. The displacement between the marker rocks ($39^{\circ} 59' .31$ N; $38^{\circ} 50' .46$ E in the east, $40^{\circ} 16' .04$ N; $38^{\circ} 51' .59$ E in the west) interpreted as similar structures on the north and south of the fault is 90 ± 5 km that cover the former total displacement value of 85 ± 5 km reported by Seymen (1975) and Şengör (1979).

Detecting the fault age is important for measuring and estimating the total displacement on fault zones. In a recent study by Boles et al. (2015), they present a new approach to identifying the source and age of paleofluids associated with low-temperature deformation in the brittle crust, using hydrogen isotopic compositions and Ar geochronology of authigenic illite in clay gouge-bearing fault zones and used this method on samples collected along the surface trace of the present NAFZ. Four of the eight collected samples are from the eastern part of the NAFZ. These samples are taken from a fault gouge in a landslide area at Koyulhisar, and an intensely altered peridotite unit on a roadcut between the towns of Koyulhisar and Reşadiye. Corresponding clay gouge ages are 24.6 ± 1.6 Ma (authigenic) and 96.5 ± 3.8 Ma (detrital) for samples taken from Reşadiye region, demonstrating a long history of meteoric fluid infiltration in the area. According to the conclusion of Boles et al. (2015)'s, today's the NAFZ incorporated preexisting, weak clay-rich rocks that represent earlier mineralizing fluid events. The meteoric fluid flow event on the east side of the sampling area is ~ 25 Ma, which shows that clay gouge present in today's NAFZ is older than modern strike-slip fault initiation.

A study by Tatar et al. (2012) provided an average fault slip rate of 23 mm/year for the eastern part of the NAFZ by using GPS vectors. The combination of the studies about the total displacement on the NAFZ is compatible with Seymen (1975) and Şengör (1979). Integration of terrestrial spectroradiometer measurement values with the SWIR detector bands of ASTER satellite data is sufficient for lithological mapping through the use of the SAM method. Remote sensing data with higher spectral resolution in the SWIR region can provide more accurate results with less similar angle values for determining different lithological classes that have similar spectral reflectance.

Resolutions are very important for such studies. The displacements at fault zones could be determined by using hyperspectral images more precisely. Depending on the spectral resolution, the number of detectable pixels that contain marker rocks increases. Furthermore, as the spatial resolution increases, the spectral classification becomes more accurate because the number of mixed pixels is reduced.

The data obtained from the spectroradiometer measurements of the object could vary regionally. In order to carry out the more precise classification, remote sensing image and spectral measurement data should be obtained at the same time.

In conclusion, optical satellite images that contain SWIR bands could be used for detecting marker rocks to determine the lateral offsets on fault zones. The combined use of the remote sensing data and geological observations released the total offset, which is 90 ± 5 km, on the NAFZ. The offset value is compatible with the value that is accepted according to previous researches.

Disclosure statement

No potential conflict of interest was reported by the authors.

Funding

This work is supported by the Scientific Research Project Fund of Cumhuriyet University [project number M-523], [project number M-614].

ORCID

- Önder Gürsoy  <http://orcid.org/0000-0002-1531-135X>
 Ziyadin Çakir  <http://orcid.org/0000-0003-3050-5619>
 Oktay Canbaz  <http://orcid.org/0000-0002-8161-1326>

References

- Abdeen MM, Allison TK, Abdelsalam MG, Stern RJ. 2001. Application of ASTER band-ratio images for geological mapping in arid regions; the Neoproterozoic Allaqlı Suture, Egypt. Abstract with Program Geological Society of America. 3:289.
- Abdülləməğlu Ş. 1959. Geology of vicinity of Alnucikdağı-Mudurnu and Göynük. İstanbul University Monographs. 1:1–94.
- Akyüz S. 2002. The surface rupture and slip distribution of the August 17, 1999 Izmit earthquake, $M = 7.4$, North Anatolian Fault. Bull Seismol Soc Am. 1:43–60.
- Armijo R, Meyer B, Hubert A, Barka A. 1999. Westward propagation of the North Anatolian Fault into the Northern Aegean: timing and kinematics. Geology. 27:267–270.
- Ayhan ME, Bürgmann R, Mcclusky S, Lenk O, Aktuğ B, Herece E, Reilinger RE. 2001. Kinematics of $Mw = 7.2$, 12 November 1999, Düzce, Turkey Earthquake. Geophys Res Lett. 28:367–370.
- Barka AA. 1981. Seismotectonic aspects of the North Anatolian fault zone [dissertation]. England: University of Bristol; p. 335.
- Barka A. 1992. The North Anatolian Fault zone. Ann Tecton. 6:164–195.
- Barka AA, Kadinsky-Cade K. 1988. Strike-slip fault geometry in Turkey and its influence on earthquake activity. Tectonics. 7:663–684.
- Bedell RL. 2001. Geological mapping with ASTER satellite: new global satellite data that is a significant leap in remote sensing geologic and alteration mapping. Spec Publ Geol Soc Nevada. 33:329–334.
- Bergougnan H. 1976. Structure of the Pontic Chain in Upper Kelkit (Northeast Anatolia). Bull Soc Geol Fr. 18:675–686.
- Blewitt G. 1993. Advances in Global Positioning System technology for geodynamics investigations. In: Smith DE, Turcotte DL, editors. Contributions of space Geodesy to geodynamics: technology (Geodynamics Series, Vol. 25). Washington (DC): American Geophysical Union; p. 195–213. ISBN 0-87590-526-9
- Boles A, van Der Pluijm B, Mulch A, Mutlu H, Uysal ITB, Warr LN. 2015. Hydrogen and $^{40}\text{Ar}/^{39}\text{Ar}$ isotope evidence for multiple and protracted paleofluid flow events within the long-lived North Anatolian Keirogen (Turkey). Geochim Geophys Geosyst. 16:1975–1987.
- Bolongaro-Crevenna A, Torres-Rodríguez V, Sorani V, Frame D, Ortiz MA. 2005. Geomorphometric analysis for characterizing landforms in Morelos State, Mexico. Geomorphology. 67:407–422.
- Bozkurt E. 2001. Neotectonics of Turkey – a synthesis. Geodin Acta. 14:3–30.
- Bozkurt E, Holdsworth BK, Koçyiğit A. 1997. Implications of Jurassic chert identified in the Tokat Complex, northern Turkey. Geol Mag. 134:91–97.
- Çakır Z, Ergintav S, Akoğlu AM, Çakmak R, Tatar O, Meghraoui M. 2014. InSAR velocity field across the North Anatolian Fault (eastern Turkey): implications for the loading and release of interseismic strain accumulation. J Geophys Res Solid Earth. 119:7934–7943. doi:10.1002/2014JB011360
- Cavalie O, Jónsson S. 2014. Block-like plate movements in eastern Anatolia observed by InSAR. Geophys Res Lett. 41:26–31.
- Dennison PE, Halligan KQ, Roberts DA. 2004. A comparison of error metrics and constraints for multiple endmember spectral mixture analysis and spectral angle mapper. Remote Sens Environ. 93:359–367.
- Dikau R. 1989. The application of a digital relief model to landform analysis. In: Raper JF, editor. Three dimensional applications in geographical information systems. London: Taylor & Francis; p. 51–77.
- Gad S, Kusky T. 2007. ASTER spectral rationing for lithological mapping in the Arabian-Nubian shield, the Neoproterozoic Wadi Kid area, Sinai, Egypt. Gondwana Res. 11:326–335.
- Gürsoy Ö, Kaya Ş. 2016. Detecting of lithological units by using terrestrial spectral data and remote sensing image. J Indian Soc Remote Sens. 1:1–11.
- Hammond EH. 1964. Analysis of properties in landform geography: an application to broad scale landform mapping. Ann Assoc Am Geogr. 54:11–19.
- Herece E, Akay E. 2003. Atlas of North Anatolian Fault (NAF). General Directore of Mineral Research and Exploration Specific Journal, Ankara. 2:61.
- Hewson RD, Cudahy TJ, Mizuhiko S, Ueda K, Mauger AJ. 2005. Seamless geological map generation using ASTER in the Broken Hill-Curnamona province of Australia. Remote Sens Environ. 99:159–172.
- Hubert-Ferrari A, Armijo R, King GCP, Meyer B, Barka AA. 2002. Morphology, displacement, and slip rates along the North Anatolian Fault, Turkey. J Geophys Res. 107:2235.



- Hubert-Ferrari A, King G, van Der Oerd J, Villa I, Altunel E, Armijo R. 2009. Long-term evolution of the North Anatolian Fault: new constraints from its eastern termination. In: van Hinsbergen DJJ, Edwards MA, Govers R, editors. Collision and collapse at Africa-Arabia-Eurasia subduction zone (Vol. 311). London: Geological Society; p. 133–154. (Special Publication).
- Iwasaki A, Fujisada H, Akao H, Shindou O, Akagi S. 2001. Enhancement of spectral separation performance for ASTER/SWIR. *Proc SPIE*. 4486:42–50.
- Iwasaki A, Tonooka H. 2005. Validation of a crosstalk correction algorithm for ASTER/SIWR. *IEEE Trans Geosci Remote Sens*. 43:2747–2751.
- Kariuki PC, van Der Meer FD, Siderius W. 2003. Classification of soils based on engineering indices and spectral data. *Int J Remote Sens*. 12:2567–2574.
- Kaya Ş. 1999. Geomorphological and geological characteristics of the North Anatolian Fault Gallipoli - Işıklar Mountain section using satellite images and digital elevation model [dissertation]. İstanbul Technical University Scientific Institute.
- Kaya Ş, Müftüoğlu O, Tüysüz O. 2004. Tracing the geometry of an active fault using remote sensing and digital elevation model: Ganos segment, North Anatolian Fault Zone, Turkey. *Int J Remote Sens*. 25:3843–3855.
- Kaypak B, Eyidoğan H. 2002. Determination of upper-crust velocity structure (1-D) of the Erzincan basin and its surroundings. 1:107–122.
- Ketin İ. 1948. On the tectonic-mechanical consequences of the great Anatolian earthquakes of the last decenions. *Geol Rundsch*. 36:77–83.
- Ketin İ. 1976. A comparison between the San Andreas and the North Anatolian Faults. *Bulletin Geol Soc Turkey*. 19:149–154.
- Khan SD, Glenn N. 2006. New strike slip faults and litho-units mapped in Chitral (N. Pakistan) using field and ASTER data yield regionally significant results. *Int J Remote Sens*. 27:4495–4512.
- Koçyiğit A. 1988. Tectonic setting of the Geyve Basin: age and total displacement of the Geyve Fault Zone. *METU J Pure Appl Sci*. 21:81–104.
- Koçyiğit A. 1989. Suşehri Basin; an active fault wedge basin. *Tectonophysics*. 167:13–29.
- Kruse FA. 2012. Mapping surface mineralogy using imaging spectrometry. *Geomorphology*. 137:41–56.
- Kruse FA, Perry SL. 2013. Mineral mapping using simulated worldview-3 short-wave-infrared imagery. *Remote Sens*. 5:2688–2703.
- Massironi M, Bertoldi L, Calafa P, Visona D, Bistacchi A, Giardino C, Schiavo A. 2008. Interpretation and processing of ASTER data for geological mapping and granitoids detection in the Saghro massif (eastern Anti-Atlas, Morocco). *Geosphere*. 4:736–759.
- Natraj V, Shia RL, Yung YL. 2010. On the use of principal component analysis to speed up radiative transfer calculations. *J Quant Spectrosc Radiative Transfer*. 111:810–816.
- Nebert K. 1962. Serpantin kitleleri arasına sıkışmış bir Neojen blokuna misal olmak üzere Alabarda (Tavşanlı) linyit bölgesi [Alabarda (Tavşanlı) lignite district as example of a block to be wedged between the masses os serpentinite]. *Bull Miner Res Explor Institute (MTA) Turkey*. 58:31–37.
- Nurlu M, Batman B, Chorowicz J, Genç MA. 1995. A geometrical approach relating to the movement mechanism of North Anatolian Fault Zone. International symposium on the geology of the Black Sea region, Ankara. 283–291.
- Okada K, Ishii M. 1993. Mineral and lithological mapping using thermal infrared remotely sensed data from ASTER simulator. In: International geosciences and remote sensing symposium “Better Understanding of Earth Environment” 93:126–128.
- Okay AI, Tüysüz O. 1999. Tethyan sutures of northern Turkey (Vol. 156). London: Geological Society; p. 475–515. (Special Publications).
- Özalaybey S, Ergin M, Aktar M, Tapirdamaz C, Biçmen F, Yörük A. 2002. The 1999 İzmit earthquake sequence in Turkey: seismological and tectonic aspects. *Bull Seismol Soc*. 92:376–386.
- Reilinger R, Mcclusky S, Vernant P, Lawrence S, Ergintav S, Çakmak R, Özener H. 2006. GPS constraints on continental deformation in the Africa-Arabia-Eurasia continental collision zone and implications for the dynamics of plate interactions. *J Geophys Res*. 111:26.
- Rowan LC, Maras JC. 2003. Lithological mapping in the Mountain Pass, California area using Advanced Spaceborne Thermal Emission and Reflection Radiometer (ASTER) data. *Remote Sens Environ*. 84:350–366.
- Rowan LC, Mars JC, Simpsons CJ. 2005. Lithological mapping of the Mordor, NT, Australia ultramafic complex by using the Advanced Spaceborne Thermal Emission and Reflection Radiometer (ASTER). *Remote Sens Environ*. 99:105–126.
- Şaroğlu F. 1988. Age and offset of the North Anatolian fault. *METU J Pure Appl Sci*. 21:1–3, 65–79.
- Şengör AMC. 1979. The North Anatolian Transform Fault. Its age offset and tectonic significance. *J Geol Soc Lond*. 136:269–282.
- Şengör AMC, Görür N, Şaroğlu F. 1985. Strike-slip faulting and related basin formation in zones of tectonic escape: Turkey as a case study. In: Biddle TR, Christie-Blick N, editors. Strike-slip deformation, basin formation and sedimentation. American Society for Economic Paleontologists and Mineralogists. 37:227–264. (Special Publication).

- Şengör AMC, Tüysüz O, Imren C, Sakınç M, Eyidoğan H, Görür LE, Pichon X, Rangin C. 2005. The North Anatolian Fault: A New Look. *Annu Rev Earth Planet Sci.* 33:37–112.
- Seymen İ. 1975. Tectonic feature of North Anatolian Fault zone in Kelkit valley section [dissertation]. Istanbul: Istanbul Technical University.
- Singh A, Harrison A. 1985. Standardized principal components. *Int J Remote Sens.* 6:883–896.
- Sipahioğlu S. 1984. Investigation of earthquake activity of North Anatolian Fault Zone and its surroundings. *Bulletin of Earthquake Research*, Ankara. 45:5–138.
- Tatar O. 1996a. Determination of extension direction in naturally deformed limestones within strike-slip fault zones using microcracks; Niksar basin (Turkey) as a case study. *Turk J Earth Sci.* 5:45–53.
- Tatar O. 1996b. Neotectonic extensional and contractional strains within Pliocene basin deposits near the NW margin of the Niksar pull-apart basin, Turkey. *Turk J Earth Sci.* 5:81–90.
- Tatar O, Gürsoy H, Koçbulut F, Kavak KŞ, Sezen TF, Polat A, Akpinar Z, Mesci L, Kiratik LO. 2006. North Anatolian Fault-1942 surface fracture of Erbaa-Niksar earthquake: New observations. ATAG-10, 2-4 November, İzmir.
- Tatar O, Piper JDA, Gürsoy H, Temiz H. 1996. Regional significance of neotectonic counterclockwise rotation in central Turkey. *Int Geol Rev.* 38:692–700.
- Tatar O, Poyraz F, Gürsoy H, Çakır Z, Ergintav S, Akpinar Z, Koçbulut F, Sezen F, Türk T, Hastaoğlu KÖ, et al. 2012. Crustal deformation and kinematics of the Eastern Part of the North Anatolian Fault Zone (Turkey) from GPS measurements. *Tectonophysics.* 518–521:55–62.
- Tatar Y. 1978. Tectonic investigations on the Erzincan-Refahiye section of the North Anatolian Fault Zone. *Hacettepe University Earthscience*, Ankara. 1–2:201–236.
- Tatar Y. 1975. Tectonic structures along the North Anatolian Fault Zone, northeast of Refahiye (Erzincan). *Tectonophysics.* 29:401–409.
- Thome K, Biggar S, Slater P. 2001. Effects of assumed solar spectral irradiance on intercomparisons of earth-observing sensors. *Proc SPIE.* 4540:260–269.
- Velosky JC, Stern RJ, Johnson PR. 2003. Geological control of massive sulfide mineralization in the Neoproterozoic Wadi Bidah shear zone, southwestern Saudi Arabia, inferences from orbital remote sensing and field studies. *Pre-cambrian Res.* 2–4:235–247.
- Vicente LE, Filho CRS. 2011. Identification of mineral components in tropical soils using reflectance spectroscopy and advanced spaceborne thermal emission and reflection radiometer (ASTER) data. *Remote Sens Environ.* 115:1824–1836.
- Walters RJ, Holley RJ, Parsons B, Wright TJ. 2011. Interseismic strain accumulation across the North Anatolian Fault from Envisat InSAR measurements. *Geophys Res Lett.* 38:L05303.
- Walters RJ, Parsons B, Wright TJ. 2014. Constraining crustal velocity fields with InSAR for eastern Turkey: limits to the block-like behavior of eastern Anatolia. *J Geophys Res Solid Earth.* 119:5215–5234.
- Yaltırak C. 2002. Tectonic evolution of the Marmara Sea and its surroundings. *Mar Geol.* 190:493–529.
- Yaltırak C, Alpar B, Yüce H. 1998. Tectonic elements controlling the evolution of the Gulf of Saros (Northeastern Aegean Sea). *Tectonophysics.* 300:227–248.
- Yaltırak C, Sakınç M, Okay FY. 2000. Westward propagation of North Anatolian Fault into the northern Aegean: timing and kinematics. *Comment. Geology.* 28:87–89.
- Yılmaz Y, Yiğitbaş E, Genç SC. 1993. Ophiolitic and metamorphic assemblages of southeast Anatolia and their significance in the geological evolution of the orogenic Belt. *Tectonics.* 12:1280–1297.
- Zabci C, Sancar T, Akyüz HS, Güneç Kiyak N. 2015. Spatial slip behaviour of large strike-slip fault belts: implications for the Holocene slip rates of the eastern termination of the North Anatolian Fault, Turkey. *J Geophys Res: Solid Earth.* 120:8591–8609.